# On the characterization of an AHF cavity radiometer and its traceability to WRR/SI

J.L.Balenzategui[1], J.De Lucas[2], J.Cuenca[1], M.Molero[1], M.C.Romero[3], F.Fabero[1], J.P.Silva[1], E.Mejuto[1], F.J.Ibañez[1]

[1] PVLab-CIEMAT. Avda. Complutense, 40. 28040 Madrid (Spain) (jl.balenzategui@ciemat.es)

[2] INTA. Ctra. Ajalvir, Km 4. 28850 Torrejón de Ardoz (Madrid, Spain)

[3] Univ. Complutense de Madrid. Facultad de Óptica y Optometría. Madrid (Spain)

## Abstract

In a complementary way to the comparison to WSG to get traceability to WRR (and consequently, to SI), a solar-type cavity radiometer can also be characterized, determining the deviations of the instrument from the ideal realization of the principle of electrical substitution and obtaining its total measurement uncertainty. This work summarizes different techniques and procedures applied for the characterization of an Eppley AHF radiometer. The approach for characterization is based on the analysis of the measurement model function of the instrument. Some results obtained from calibration and testing (voltmeter, area of the precision aperture, resistance of the leads, non-equivalence factor), and from numerical simulation (effective absorptance, scattering) are presented. According to these results, current value of standard uncertainty for this instrument is about 0.42% but it is expected that further improvements in the equipment and tests can reduce this figure below 0.1% (1000 ppm) in the near future.

## 1 Introduction

Solar-type cavity radiometers, also known as *absolute cavity radiometers* (ACR) in the field of solar irradiance radiometry (CIMO-VII 1977, Fröhlich and London 1986, Frölich 1991), are instruments with the highest metrological level for the measurement of the solar Direct Normal Irradiance (DNI). Cavity radiometers work under the *Principle of electrical substitution* or *compensation*, or *Principle of equivalence* (Hengstberger 1989, Fox and Rice 2005), so radiant power becomes directly linked to electrical power (given in Watts in SI), which is more easily and accurately measured.

The common practice for calibration of an ACR is by direct comparison to another standard reference cavity radiometer under natural sunlight in outdoor conditions (CIMO 2017). This is usually carried out during International Pyrheliometer Comparisons (IPC), in which radiometers from institutions all around the world are compared to a special group of ACRs, the World Standard Group (WSG), designated by WMO to materialize the World Radiometric Reference WRR (CIMO-VII 1977, Finsterle 2016). Despite WRR scale is based on an 'artifact' or 'prototype', it is recognized by consensus as the primary reference of solar irradiance, and every radiometer in WSG is considered as the practical realization (*mise en practique*) of the $W \cdot m^{-2}$ unit.

Additionally, traceability to WRR (ideally) provides direct traceability to SI units, which has been periodically checked in intercomparisons between WRR and SI radiometric scales (Romero et al. 1991, 1995, Finsterle et al. 2008, Fehlmann et al. 2012).

In an alternative or complementary way, ACRs can also be calibrated by *characterization* (Brusa and Fröhlich 1986, Finsterle 2008), this is, by a set of laboratory calibrations, independent tests and model/numerical simulations of its individual components, identifying and quantifying the sources of error in the measurements, and calculating the total uncertainty of the instrument (NIST 2021). Characterization was considered from the very moment of defining the WRR as a requirement for the *absolute radiometers* in order to determine its accuracy and reliability (CIMO-VII 1977). There are several examples of characterization of ACRs in the literature, mainly for instruments involved in the measurement of Total Solar Irradiance (TSI) on spacecraft (Balenzategui et al 2022).

In any case, both *comparison to WSG* and *characterization* are means to get traceability to SI units. Figure 1 illustrates this double way. But, except for the manufacturers and designers of the ACR, it is very difficult for an independent laboratory to undertake the task via characterization, and application of the first method is preferred due to its greater simplicity. Such is the technical complexity of characterization (even risky because of the delicate manufacture of the cavities) that it is generally considered not worth it.

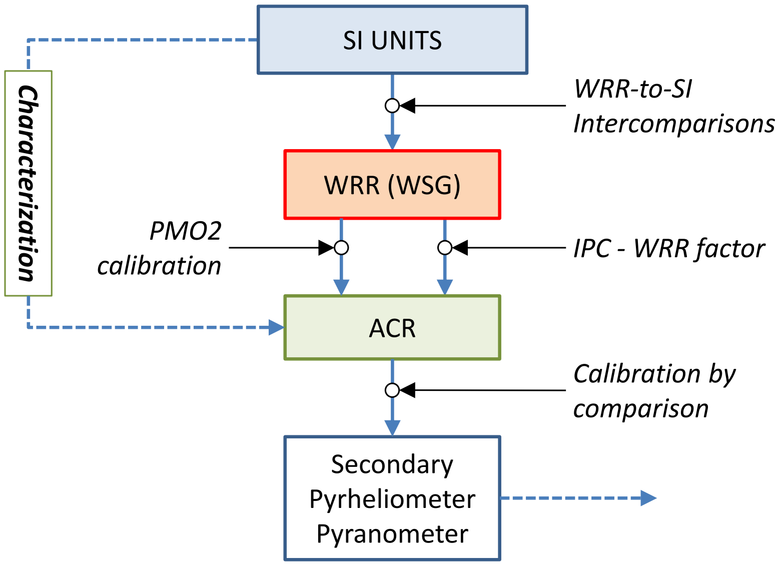


**Figure 1. Flow chart illustrating the usual procedure for getting SI traceability of a cavity radiometer through WRR and the alternative process of characterization.**

Despite that research task can be so challenging, PVLab-CIEMAT, in close collaboration with INTA, has been involved in the characterization of two commercial ACRs that constitute the reference for the calibration of their solar irradiance secondary standards: an AHF (Automatic Hickey-Frieden) radiometer, by Eppley Labs (USA), and a PMO6 radiometer, by Davos Instruments and PMOD (CH).

This work describes the different techniques applied to the characterization of the AHF radiometer and some of the results obtained up to now. A first sight about the general procedure of characterization is given. The physical characteristics and mode of operation of AHF are described next. After, a summary of the characterization results of the different parameters of interest is given and the standard uncertainty of the measurements taken with the instrument is calculated. Some important aspects about the characterization are finally discussed and highlighted.

## 2 Characterization of a cavity radiometer

Figure 2 schematically shows the basic process of ACR characterization. Like for any other meter or sensing instrument, characterization of an ACR must be based in its *measurement model function*, which relates the magnitude $y$ to be determined with a series of input variables (measured during its operation) and a set of known parameters (characteristic constants of the instrument), $y = f(x_1, x_2, \ldots, x_N)$, and not containing empirical factors. For example, in a simple or idealized measurement model of an ACRs, the magnitude of interest is the solar DNI irradiance *E*, an input variable being measured could be the electrical power $P_E$ (giving the unit of W) and the area *A* of the precision aperture would be a constant parameter (giving the unit of $m^2$). In the particular case of ACRs, general guidelines for their characterization and the correction factors to take into account were already suggested by WMO CIMO (CIMO-VII 1977, Recommendation 4, Annex V) more than 40 years ago.

The measurement function is common for all the instruments of a given model of ACR (of a given manufacturer), but the value of the constants are, in general, specific to each particular instrument. And instruments created by different manufacturers (with different methods of operation, technologies and components) have different model functions.

Then, first step is the definition of this measurement model function and the identification of these variables and parameters. Alternatively, when a function cannot be clearly defined, it is necessary to know the procedure or the sequence of steps applied for the determination of the magnitude $y$. Then, the characterization task involves, on the one hand, the calibration of the measurement devices (in the former example, a power meter or a multimeter measuring current and voltage). And, on the other hand, the determination or estimation of the characteristic parameters: some of them might be directly measured or calibrated (as the area of the precision aperture), while other could require modelling, simulation, or numerical computation, or even a mixture between indirect measurements and modelling. And each input quantity $x_i$ have to be determined with its associated uncertainty $u_i$. Calibration of input quantities links them to SI units by means of reference standards (e.g. to units of temperature, current, voltage, area, etc).

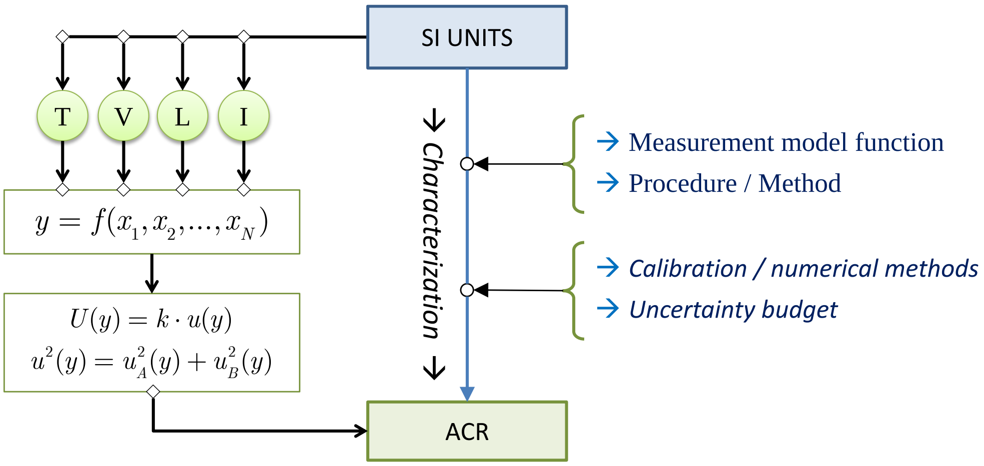


**Figure 2 Diagram summarizing the characterization process of a cavity radiometer according to the approach described in this work. T,V,L,I stand for the magnitudes and units of temperature, voltage, length (area) and electrical current.**

A final uncertainty budget has to be evaluated, considering all the contributions of the input variables and parameters, and whenever possible, according to the principles of the JCGM 100:2008 or *GUM* guide (BIPM 2008). In this step it is important to obtain the sensitivity coefficients $s_i$ with which each particular contribution $u_i$ to overall uncertainty $U$ has to be accounted for, in the form: $U^2 = \sum(s_i^2 \cdot u_i^2)$.

# 3 Fundamentals of AHF radiometer

## 3.1 Structure and operation of the AHF radiometer

The HF is a passive-type cavity radiometer, originally developed by J.R.Hickey and R.G.Frieden in Eppley Labs in the mid-1970s for the Nimbus satellite series (Hickey et al 1977). First terrestrial versions were sold in 1977 (Zerlaut 1982). *Automatic* versions (AHF) were developed in the early 2000s.

The sensor of the (A)HF is created by two twin cavities attached to opposite sides of a wire-bound thermopile wrapped in a toroidal structure (see Figure 3). The rear cavity is open to a blackbody-like hollow aluminum block at ambient temperature, while the front cavity receives sunlight. This creates a balanced or compensated detector (Hickey et al 1977). The sunlight enters the front cavity through a collimator tube reducing the FOV up to 5°, and a precision aperture of known area $A$. Cavities are created by an inverted cone within a cylinder, internally coated by Chemglaze (Aeroglaze) Z302 black glossy paint.

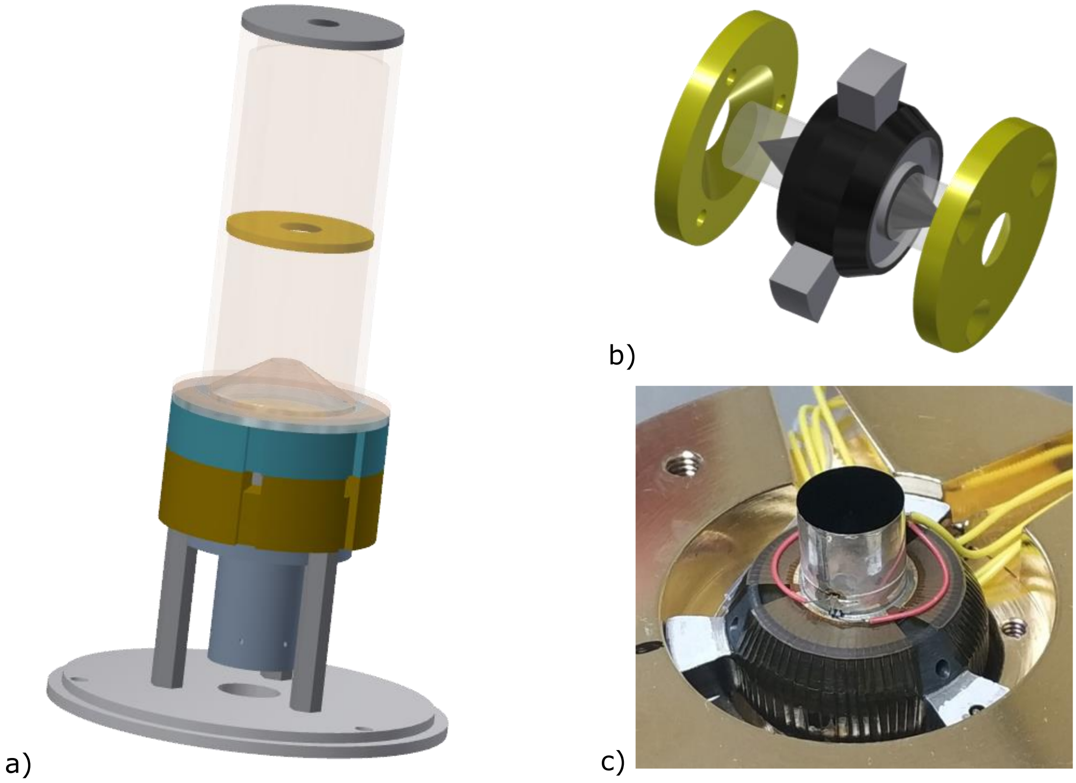


**Figure 3. Structure of AHF radiometer: a) internal view (false colored) of the collimator tube and its baffles, the block containing the cavity and the rear blackbody; b) model of the sensor formed by the twin cavities attached to the wire-bound thermopile and the precision apertures; c) a real picture of the AHF front cavity, thermopile and connections.**

The heater wire is internally wound in the cone and partially in the cylinder, in order to reproduce radiative heating location and amount (and a better equivalence between electrical and radiative heating). The cavity heater is connected in a 4-wire Kelvin scheme, and heater voltage $V_H$ and current $I_H$ are measured with an external 34970A datalogger to obtain the electrical power $P_E$ ($I_H$ is obtained from the voltage drop $V_I$ in a shunt resistor $R_N$). The small power loss in the thin wires connecting the heater is estimated from their resistance $R_C$. The front cavity is periodically occluded from sunlight by an electromechanical shutter (closed phase) in order to measure the voltage output $V_{TE}$ of the thermopile when electrically heated, and also the thermopile offset signal $V_{T0}$ when cavity is not subjected to any excitation. During open phases, the voltage output $V_{TS}$ of the thermopile produced by the Sun radiative power is measured every 30 seconds.

## 3.2 The AHF measurement model function

The generated emf in the thermopile is directly proportional to the (electrical, radiant) power heating the front cavity. The radiant power reaching the cavity would be given by:

$$P_S = A \cdot \alpha_C \cdot \gamma \cdot E \qquad \rightarrow \qquad V_{TS} - V_{T0} = k_S \cdot P_S \tag{1}$$

where $E$ is the direct normal irradiance, $\alpha_C$ is the effective absorptance of the cavity and $\gamma$ is a *stray-light factor* (Hickey et al 1977, Karoli et al 1983) associated to the collimator and baffles, while $k_S$ is a proportionality constant (slope of a straight line). On the other hand, electrical power is calculated by:

$$P_E = I_H V_H - I_H^2 R_C \qquad \rightarrow \qquad V_{TE} - V_{T0} = k_E \cdot P_E \tag{2}$$

being $k_E$ a proportionality constant too. According to the *Principle of Electrical Substitution*, if excitation (radiant, electrical) powers are equivalent or indistinguishable to the effect of heating the cavity, the response of the system will be the same. In that case:

$$\frac{V_{TS} - V_{T0}}{P_S} = \frac{V_{TE} - V_{T0}}{P_E} \qquad \rightarrow \qquad k_S = k_E \tag{3}$$

However, imperfections in the practical realization of this principle can produce slight differences in the system output, so then:

$$k_S \neq k_E \qquad \rightarrow \qquad L = k_E / k_S \tag{4}$$

being $L$ named the *non-equivalence factor*. Finally, combining equations (1)–(4), solar irradiance is calculated by AHF as:

$$\begin{aligned} E &= \frac{L}{A\alpha_C \gamma} \cdot \left( \frac{V_{TS} - V_{T0}}{V_{TE} - V_{T0}} \right) \cdot I_H \left( V_H - I_H R_C \right) \\ &= \frac{L}{A\alpha_C \gamma} \cdot \left( \frac{V_{TS} - V_{T0}}{V_{TE} - V_{T0}} \right) \cdot \frac{V_I}{R_N} \left( V_H - \frac{V_I}{R_N} R_C \right) \end{aligned} \tag{5}$$

This is the measurement model function of the AHF cavity radiometer, making $E$ explicitly dependent on 11 input variables: $E = f\ (A,L,\alpha_C,\gamma,V_{TE},V_{TS},V_{T0},V_H,V_I,R_N,R_C)$. In this function, operative-type input variables (electrical signals measured during operation of the radiometer $V_{TE}$, $V_{TS}$, $V_{T0}$, $V_H$, $V_I$) and characteristic parameters ($A$, $L$, $\alpha_C$, $\gamma$, $R_N$, $R_C$, ideally constant) can be identified. First group requires the calibration of the instrument(s) measuring them, while second group needs the calibration or estimation (numerical models) of their values.

# 4 Characterization results

A summary of the methods and techniques used for the characterization of every input variable and parameter is given next. The test and/or reference values for evaluating them and for calculating their uncertainty contribution are indicated, and later collected in section 5.2. Further details about the techniques and applied methods can be found elsewhere (Balenzategui et al, 2022).

## 4.1 Calibration of DVM (datalogger)

Internal voltmeter (DMM) of the 34970A datalogger was calibrated in the *Electricity Laboratory* of *Centro de Metrología y Calibración* (INTA). Calibration mainly covered voltage measurements (100 mV, 1V and 10 V ranges). Reference values for calculating uncertainty of every term in section 5.2 are the average values measured by the instrument in outdoor operation (calibration campaigns) in the period 2015-2018. Net uncertainty of voltage signals is obtained as: $u^2(V_X) = u^2(V_{SP}) + u^2(V_{CAL})$, including contributions from DMM calibration uncertainty ($V_{CAL}$) and DMM accuracy specifications ($V_{SP}$).

## 4.2 Calibration of the precision aperture area

Precision apertures of ~8 mm diameter with an internal chamfer are carefully drilled on disks made of Invar, 4 mm thick, and have a nominal area of 50 $mm^2$. Their areas (front and rear, even though this second is not used in the model function) were calibrated in the *Laboratory of Length and Precision Engineering* of the *Centro Español de Metrología* (CEM, the Spanish NMI). First step was to measure the aperture by means of a vision machine with a resolution of 0.1 µm, traced to SI. A total of 360 points distributed along the perimeter of the opening were resolved, that were approached to a circumference by a least-squares fitting, obtaining the radius and the location of the center. The area was determined by adding the surfaces of the triangles created between two consecutive points in the border of the aperture and the center of the circumference calculated in the previous step. This method is equivalent to that applied by PTB in circular apertures for radiometric applications (Neugebauer et al 2015). The area of the front aperture so calculated was $A$ = (50.183 ± 0.015) $mm^2$ ($k$=2).

## 4.3 Calibration of shunt resistance $R_N$

A wire wound power 4-terminal axial shunt resistor is used for measuring the current $I_H$ supplied into the AHF cavity heater. It is placed inside the control unit of the instrument, and has a nominal value of $R_N$ = 10 Ω (±0.01%), max rated power of 2W and temperature coefficient of ±15ppm/°C (datasheet values).

Shunt resistor was calibrated at a room temperature of (23 ± 1) °C, also in the *Electricity Laboratory* (INTA), at an intensity of 17.5 mA. This current was selected by considering the statistical distribution of electrical powers supplied into the heater resistance (of around ~150 Ω) during calibration phases in normal operation of the radiometer. At this current, shunt resistor dissipates around 3 mW so self-heating effects are negligible. The certified value of $R_N$ was (9.998 69 ± 0.000 11) Ω, ($k$ = 2).

## 4.4 Calibration of wires' resistance $R_C$

The wires resistance $R_C$ was carefully measured in the PVLab-CIEMAT by means of a calibrated Keysight 34420A micro-ohmeter with a resolution of 7½ digits. The wires were contacted in a 4-point configuration with paired in-line *Accuprobe* tips (K-type Z-adjustable probe tips, reference IK2C8C3D). Total resistance is obtained as the sum of the resistances of every branch (from positive contact point to cavity, and from cavity to negative contact point), giving a total $R_C$ = (50.9907 ± 0.0067) mΩ (k=2) as result.

## 4.5 Estimation of the optical scattering factor $\gamma$

The scattering factor $\gamma$ was estimated by means of Zemax Optics Studio simulation program working in non-sequential mode (ray tracing model). A simplified model of the collimator with the real dimensions of apertures and distances was built thanks to the Zemax design tools (see Figure 4). Inner cylinder tube and baffles are also painted with Chemglaze Z302 while internal face of the last baffle with a truncated-cone shape is painted with Nextel. Spectral reflectance of these coatings (hemispherical and specular components) and of the precision aperture surface (Invar) were experimentally measured in a Perkin Elmer Lambda 900 spectrophotometer and their solar spectrally-weighted reflectance factors (diffuse, specular) were computed. Sun was simulated as a double diffuse lambertian source considering the central solar disk and the aureole region, with diameters defined in terms of the distance to, the angular apertures and FOV of the collimator. The spectral distribution of sunlight was also incorporated into the specifications of this double source by using the ASTM G-173-03 *Reference Solar AM1.5 Spectral Irradiance* (NREL 2021).

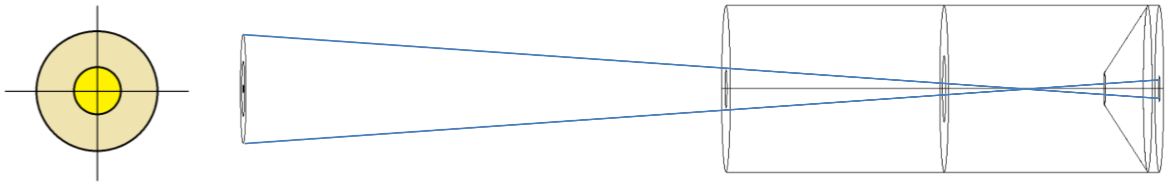

**Figure 4. Simulation of scattering effects due to collimator and its internal baffles into the irradiance reaching the AHF cavity. Source simulating the Sun (on the left) includes two regions (solar disk and aureole region).**

For estimating the scattering factor, the amount of power reaching a detector placed behind the aperture area was computed with and without the collimator, and the ratio between these powers calculated. The ray tracing simulation was run 15 times for each case (w/ and w/o collimator) for obtaining average and standard deviation values.

**Table 1. Estimation of the optical scattering factor $\gamma$ by ray tracing simulation with Zemax Optics Studio.**

| *Average power w/o collimator* | *Average power with collimator* | *N* | *γ (ratio)* | *σ* |
|---|---|---|---|---|
| 3.6890 W | 3.6933 W | 15 | 1.001 17 | 0.000 98 |

The value obtained in the ray tracing simulation agrees quite well with that provided by the manufacturer as the *Approximate Stray Light Correction Factor* in the instrument fact sheet: $\gamma$ = 1.0010 (0.1%). However, a value of uncertainty is still pending to be calculated for our ray tracing simulation results. For this reason, the original values given by the manufacturer were used for the uncertainty budget in this work (considering the 0.1% uncertainty is given with a coverage factor $k$=2). This figure is supposed to be very close to the one that will be obtained in our research.

## 4.6 Estimation of effective absorptance

Effective integrated normal absorptance has been calculated by the *method of sums* (Bedford and Ma 1974) by considering the solar radiation reaching the cavity only in the direction of its optical axis through the precision aperture (placed normal to this axis). The cylinder and cone are divided into sections, normal to the optical axis, and local values of effective absorptance are calculated in each (see Figure 5). Both the shape and the optical properties of the coating determine the absorptivity $\alpha_C$ of the cavity.

Reflectance $\rho$ of the Z302 glossy paint has both specular $\rho_S$ and diffuse $\rho_D$ components, values in the range $\rho_S$ ~ 0.050-0.065 and $\rho_D$ ~ 0.007-0.010 (Fox and Rice 2005, Patrick et al 2016, Jung et al 2015). Thus, reflected radiation in each section is assumed to have two contributions: a) *diffuse type*: after the first initial reflection in the cone, radiation can well exit from the cavity through the aperture or well be totally absorbed by the walls of the cylinder section, without additional reflections; b) *specular type*: the light beam keeps the specular behavior in successive bounces and, after 5 consecutive internal reflections, its contribution is totally absorbed.

Finally, $\alpha_C$ is calculated by integration of the local effective absorptance values over the cone region being illuminated by sunlight, reaching the precision aperture in normal direction. Results for the local effective absorptance are shown in Figure 5. Uncertainty $U(\alpha_C)$ was obtained by the Monte Carlo method by varying in small amounts the geometrical parameters as well as the reflectance of the cavity. This way, a value of $\alpha_C$ = (0.999 12 ± 0.000 11) was obtained for a coverage factor of 95%.

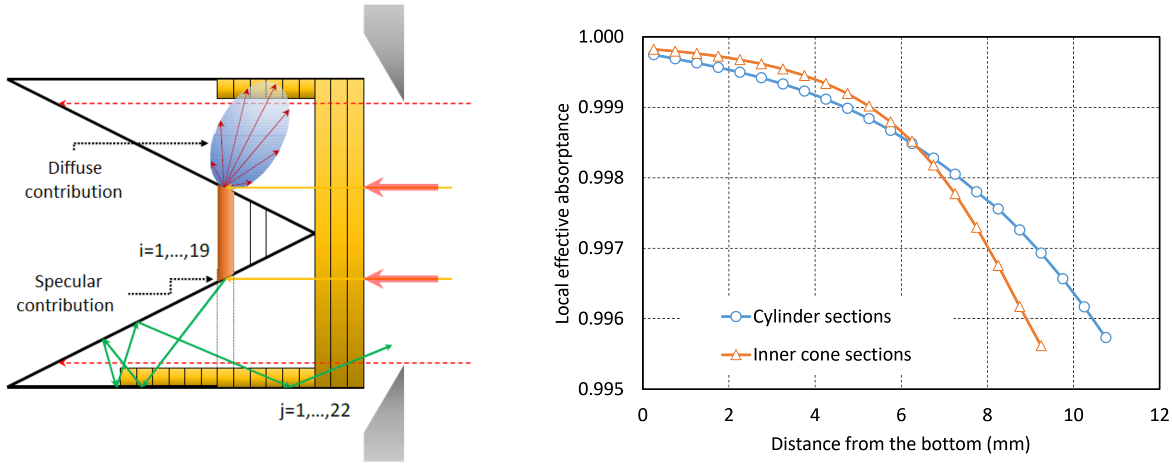


**Figure 5. Estimation of effective absorptance of the AHF cavity: (left) approach for calculation by dividing the cavity wall and cone in sections; (right) results of the local values of effective absorptance in every section.**

These results are consistent to those later obtained by ray tracing simulation in Zemax Optics Studio. In this case, slightly different reflectance values of Z302 ($\rho_S$ = 0.039, $\rho_D$ = 0.017, experimentally determined) were used, which resulted in a little lower absorptance of the cavity (see Table 2). In these ray tracing simulations, it was confirmed that only diffuse component escapes from the cavity.

**Table 2. Estimation of effective absortance of the cavity, and relative irradiance distribution between cone and cylinder. $\rho_S$ | $\rho_D$ stand for the values of specular and diffuse reflectance used for Chemglaze Z302 in the simulations. The amount of irradiance absorbed in the cylinder and in the cone is also calculated.**

| *Illumination source* | *Method* | $\rho_S$ \| $\rho_D$ | *Absorptance* | *Reflectance* | *Cone* | *Cylinder* |
|---|---|---|---|---|---|---|
| Non selective | Sums | 0.057 \| 0.009 | 0.999 12 | 0.000 88 | 94.3% | 5.7% |
| Monochromatic (λ = 550 nm) | Zemax | 0.039 \| 0.017 | 0.998 33 | 0.001 67 | — | — |
| Sun | | | 0.998 28 | 0.001 72 | 94.4% | 5.6% |

## 4.7 The non-equivalence factor *L*

The materialization of the Principle of electrical substitution in AHF system is realized in terms of *equalizing powers* instead of *equalizing temperatures* (or thermal flux) between open (radiant) and closed (electrical) phases. This approach works fine because of the extremely linear dependence of thermopile output voltage on any of the excitation powers.

Considering this realization, it has been proposed (Balenzategui et al, 2022) to use the own definition of the non-equivalence factor $L$ for determining its value. For this purpose, the slopes $k_E$, $k_S$ of the straight lines in (1) and (2) are calculated by a least squares fit and the ratio (4) is computed. The uncertainty of $L$ is next calculated by Monte Carlo method.

For the application of this procedure, it is important that thermopile output signals be measured with the same instrument (DVM) than in normal operation (not external meters), and during the same time period for having similar working conditions in open/closed cycles. And a standard for setting reference $P_S$ values is required. For this reason, the data collected by our AHF during IPC-XII (2015) were used for a first evaluation of this method.

Results are shown in Table 3. As expected, non-equivalence factor is very close to 1 and the correction introduced by *L* into (5) is very small. However, the resulting uncertainty (0.42%, *k*=2) is relatively high, mainly due to the contribution of the measurement of voltages by the DVM.

**Table 3. Results of the determination of the $k_S$, $k_E$ slopes and of the non-equivalence factor *L*. Uncertainties have been calculated by Montecarlo method.**

| *Parameter* | *Value* | *Uncertanty (k=2)* |
|---|---|---|
| $k_S$ (mV/W) | 22.607 46 | 0.102 90 (0.46%) |
| $k_E$ (mV/W) | 22.610 52 | 0.032 01 (0.14%) |
| *L* | 1.000 135 | 0.004 768 (0.48%) |

# 5 Uncertainty budget

The method for uncertainty evaluation follows the guidelines from the JCGM 100:2008 or *GUM* guide (BIPM 2008). First, general approach and concepts are posed. After, explicit calculation of uncertainty for AHF radiometer is given.

## 5.1 General approach for computation of uncertainty

The objective is the calculation of the *expanded* uncertainty *U*(*E*) of the solar irradiance measured by the radiometer, which is expressed by applying a coverage factor *k* to the *net combined standard uncertainty u*(*E*) as:

$$U(E) = k \cdot u(E) \tag{6}$$

It is a common practice to use *k*=2 which, for a normal distribution, corresponds to a confidence interval of 95.45% (*k*=1 for 68.27%). According to GUM, the net combined standard uncertainty *u*(*E*) of the irradiance *E* would be given by:

$$u^2\left(E\right) = u_A^2\left(E\right) + u_B^2\left(E\right) \tag{7}$$

being $u_A(E)$ the A-type contribution, due to the dispersion of measured values around the mean, of stochastical nature, and $u_B(E)$ the B-type contribution, due to systematic sources of deviation in measurement.

A-type uncertainty $u_A(E)$ is usually computed from a set of *N* experimental data points, treated as they were scattered according to a normal distribution, as:

$$u_A^2\left(E\right) = \frac{\sigma^2\left(E\right)}{N} = \frac{1}{N\left(N-1\right)} \sum_{i=1}^{i=N} \left(E_i - \mu\right)^2 \tag{8}$$

being *μ* the mean and *σ*(*E*) the standard deviation of the individual irradiance values $E_i$ taken as valid. However, in this particular case, the A-type contribution will not be considered because the (varying) solar irradiance is measured by AHF only once, at periodic intervals in normal outdoor operation. Additionally, it can be considered as regrettably compared to B-type contribution.

B-type uncertainty $u_B(E)$, assuming in general that the magnitude under evaluation $y$ is a function of several input independent variables, $y = f(x_1, x_2, \ldots, x_N)$, is calculated as:

$$u_B^2(y) = \sum_{i=1}^{n} \left[ \frac{\partial f}{\partial x_i} \right]^2 u^2(x_i) + 2 \sum_{i=1}^{n-1} \sum_{j=i+1}^{n} \frac{\partial f}{\partial x_i} \frac{\partial f}{\partial x_j} u(x_i, x_j) \tag{9}$$

being $u(x_i)$ the standard uncertainty of the input variable $x_i$, and $u(x_i,x_j)$ the estimated covariances of $x_i$ and $x_j$. When input values are not correlated $u(x_i,x_j) = 0$. The partial derivatives in (9) are called *sensitivity coefficients*. Additionally, depending on its nature or origin, every uncertainty term $u(x_i)$ is associated to a specific statistical distribution (normal, rectangular, triangular, trapezoidal, etc) and weighted with a corresponding factor (e.g. $1/\sqrt{3}$ for a rectangular distribution).

## 5.2 B-type uncertainty of the AHF irradiance measurements

In our case, and neglecting correlation terms, the B-type uncertainty will be:

$$u_B^2\left(E\right)=\sum_{i=1}^{n}\left[\frac{\partial f}{\partial x_i}\right]^2 u^2\left(x_i\right) \tag{10}$$

where $f$ is now the measurement model function (5). For practical reasons, it is better to calculate *relative uncertainty* in the form:

$$\frac{u_B^2(E)}{E^2}=\sum_{i=1}^{n}\frac{1}{E^2}\left[\frac{\partial f}{\partial x_i}\right]^2 u^2(x_i) \tag{11}$$

Expanding the dependences of the model function $f$ we get:

$$\begin{aligned}\frac{u_B^2\left(E\right)}{E^2}&=\frac{1}{E^2}\left[\frac{\partial f}{\partial L}\right]^2 u^2\left(L\right)+\frac{1}{E^2}\left[\frac{\partial f}{\partial A}\right]^2 u^2\left(A\right)+\frac{1}{E^2}\left[\frac{\partial f}{\partial \gamma}\right]^2 u^2\left(\gamma\right)\ldots\\&+\frac{1}{E^2}\left[\frac{\partial f}{\partial \alpha_C}\right]^2 u^2\left(\alpha_C\right)+\frac{1}{E^2}\left[\frac{\partial f}{\partial V_{TE}}\right]^2 u^2\left(V_{TE}\right)+\frac{1}{E^2}\left[\frac{\partial f}{\partial V_{TS}}\right]^2 u^2\left(V_{TS}\right)\ldots\\&+\frac{1}{E^2}\left[\frac{\partial f}{\partial V_{T0}}\right]^2 u^2\left(V_{T0}\right)+\frac{1}{E^2}\left[\frac{\partial f}{\partial V_H}\right]^2 u^2\left(V_H\right)+\frac{1}{E^2}\left[\frac{\partial f}{\partial V_I}\right]^2 u^2\left(V_I\right)\ldots\\&+\frac{1}{E^2}\left[\frac{\partial f}{\partial R_C}\right]^2 u^2\left(R_C\right)+\frac{1}{E^2}\left[\frac{\partial f}{\partial R_N}\right]^2 u^2\left(R_N\right)\end{aligned} \tag{12}$$

and calculating the partial derivatives of the measurement model function (5), equation (12) becomes:

$$\begin{aligned}\frac{u_B^2(E)}{E^2}&=\frac{1}{L^2}u^2\left(L\right)+\frac{1}{A^2}u^2\left(A\right)+\frac{1}{\alpha_C^2}u^2\left(\alpha_C\right)+\frac{1}{\gamma^2}u^2\left(\gamma\right)\ldots\\&+\frac{u^2\left(V_{TE}\right)}{\left(V_{TE}-V_{T0}\right)^2}+\frac{u^2\left(V_{TS}\right)}{\left(V_{TS}-V_{T0}\right)^2}+\frac{\left(V_{TS}-V_{TE}\right)^2}{\left(V_{TE}-V_{T0}\right)^2\left(V_{TS}-V_{T0}\right)^2}u^2\left(V_{T0}\right)\ldots\\&+\frac{1}{\left(V_H-\dfrac{V_I}{R_N}R_C\right)^2}\left[u^2\left(V_H\right)+\left(\frac{V_I}{R_N}\right)^2 u^2\left(R_C\right)+\left(V_H-2\frac{V_I}{R_N}R_C\right)^2\left(\frac{u^2\left(V_I\right)}{V_I^2}+\frac{u^2\left(R_N\right)}{R_N^2}\right)\right]\end{aligned} \tag{13}$$

The key aspect to be highlighted here is that uncertainty contribution of every input variable $u(x_i)$ is weighted by its corresponding sensitivity coefficient.

By using this expression (13), with the values of the input variables obtained during the AHF characterization and the sensitivity coefficients, a final figure of relative uncertainty $u_B(E)$ = 4224×$10^{-6}$ ($k$=1) is obtained, as detailed in Table 4. The optical quality factor $\gamma$ is the only term still based on the data provided by the manufacturer.

**Table 4. Calculation of uncertainty components for AHF solar irradiance measurements on the basis of its measurement model function.**

| *Term* | *Estimate Test value* | *Uncertainty (k=1)* | *Sensitivity coeff. S / E* | *Contribution (×$10^{-6}$)* | *Relative contribution* |
|---|---|---|---|---|---|
| $L$ | 1.000 135 | 0.002 384 | 0.99986 | 2383.4 | 31.84 % |
| $A$ | 50.183 mm$^2$ | 0.007 5 mm$^2$ | 0.019927 mm$^{-2}$ | 149.5 | 0.13 % |
| $\alpha_C$ | 0.999 12 | 0.000 06 | 1.0009 | 61.2 | 0.02 % |
| $\gamma$ | 1.001* | 0.000 5* | 0.9990 | 500.0 | 1.40 % |
| $V_{TE}$ | 0.956 152 mV | 0.002 344 mV | 1.0452 mV$^{-1}$ | 2449.8 | 33.64 % |
| $V_{TS}$ | 0.966 129 mV | 0.002 344 mV | 1.0344 mV$^{-1}$ | 2424.9 | 32.96 % |
| $V_{T0}$ | -0.624 680 µV | 0.002 338 mV | 0.010786 mV$^{-1}$ | 24.9 | 0.00 % |
| $V_H$ | 2.508 384 V | 0.000 081 V | 0.39884 V$^{-1}$ | 32.2 | 0.01 % |
| $V_I$ | 0.166 645 V | 0.000 0081 V | 5.9981 V$^{-1}$ | 48.4 | 0.01 % |
| $R_C$ | 50.990 7 mΩ | 0.003 4 mΩ | 6.6464×$10^{-3}$ mΩ$^{-1}$ | 0.022 | 0.00 % |
| $R_N$ | 9.998 69 Ω | 0.000 055 Ω | 0.099956 Ω$^{-1}$ | 5.5 | 0.00 % |
| | | | Total $u_B$ ($k$=1) | 4224 | 100.0 % |

*value originally given by the manufacturer.

## 6 Discussion

With the exception of the optical factor $\gamma$, the rest of the input quantities in the AHF measurement model function have been fully characterized with its uncertainty. Many other complementary tests for an in-deep knowledge of the sensor, of the control electronics and of the system operation as a whole have also been carried out, although are not described here.

However, despite the huge effort involved in the characterization, there are some aspects that need to be further studied and analyzed.

One of the most critical aspects is the determination of the non-equivalence factor *L*. First, because it supposes the highest contribution to the overall uncertainty and reducing this contribution should be one of our main objectives. Second, because the proposed method seems to make the irradiance measured by AHF to be dependent on a given radiant source (Sun) and on a reference instrument determining its radiant power (WSG). Thus, the value of *L* so determined would only be valid for comparison to WRR scale. So the method would need to be developed and improved to clarify these aspects. It is also pending of a comparison against trap detectors and/or cryogenic radiometers of the SI lab scale in collaboration to IO-CSIC (DI of the Spanish NMI for radiometry quantities) to verify the value of $L$ and the validity of the approach. It would also be convenient to look for alternative methods of determination of $L$, maybe through experiments in a vacuum chamber to evaluate the effect of air convection.

Contributions of similar relative weight are due to measurements of thermopile output, $V_{TE}$, $V_{TS}$, also contributing into the current $L$ figure. A new micro-voltmeter specific for readings of the thermopile voltages, with a better match between the range or full scale value and the thermopile signals, and better resolution and accuracy, would be required.

Diffraction effects in AHF are also a subject to be better studied, both experimentally and by simulation (Zemax). Preliminary results have given evidence that these diffraction effects are present and affect in some extent the irradiance values measured by AHF. This is of importance because, to date, this effect has not been considered for the AHF instrument in the literature.

The additional question of key importance refers to the traceability of the AHF irradiance measurements to WRR/SI scales, and not only how large is the uncertainty obtained from characterization. It is expected that corrected/improved values of the input quantities for the model function will produce refined DNI values as a consequence. A detailed evaluation of the DNI values measured by AHF during IPC-XIII (with and without using these corrected values) and their comparison to reference WSG irradiance will give a valuable information about the deviation of AHF with respect to the WRR scale in each case. Comparison to trap detectors and/or cryogenic radiometers will also serve as a check for the evaluation of the characterization results in terms of the AHF traceability to the SI lab scale.

# 7 Conclusions

This work has described the procedure and results obtained to date in the characterization of an Eppley AHF cavity radiometer. The input quantities in its measurement model function have been identified, and they have been subjected to calibration and estimation (by experimental and numerical methods). The different techniques and procedures applied have been described in short, and the individual contribution of uncertainty from each component has been estimated.

As a global result, current figure of B-type uncertainty for this instrument is of ~0.42% ($k$=1). Reducing the uncertainty of the AHF irradiance measurements below the threshold of $1000\times10^{-6}$ (0.1%, 1000 ppm) is the goal to be achieved in the next steps of our research. Some of the issues to be addressed in the near future, already pointed out in the work (as the contributions due to $L$, $V_{TE}$, $V_{TS}$), make this goal quite realistic.

# Acknowledgements

This work has been partially funded by the "Ministerio de Industria, Economía y Competitividad" through the "Programa Estatal de Fomento de la Investigación Científica y Técnica de Excelencia – Subprograma de Generación del Conocimiento". Project title: "Desarrollo de Patrones Primarios de Irradiancia Solar Basados en Radiómetros Absolutos de Cavidad (DEPRISACR)", reference CGL2017-87299-P.

References to commercial equipment, instruments, or materials in this paper are only given for descriptive purposes, in order to clarify the procedures be described adequately. Such references do not imply any recommendation or endorsement by any of the companies (CIEMAT, INTA, UCM), nor it is intended to imply any qualification about the quality of the equipment.

# References

Balenzategui JL, De Lucas J, González-Leiton A, Cuenca J, Molero M, Fabero F, Silva JP, Mejuto E, Muñoz R, Arce A, Prieto E, 2022a: Characterization of Absolute Cavity Radiometers for traceability to SI of solar irradiance. To be sent to Measurement Science and Technology (in preparation).

Balenzategui JL, Molero M, Silva JP, Fabero F, Cuenca J, Mejuto E, De Lucas J, 2022b: Uncertainty in the calibration transfer of solar irradiance scale: from absolute cavity radiometers to standard pyrheliometers. Sent to Solar (MDPI editorial, manuscript ID solar-1555740). Pending of acceptance.

Bedford RE, Ma CK, 1974: Emissivities of diffuse cavities: Isothermal and nonisothermal cones and cylinders. Journal of Optical Society of America 64, 339-349

BIPM, IEC, IFCC, ISO, IUPAC, IUPAP and OIML 2008, Evaluation of Measurement Data Guide to the Expression of Uncertainty in Measurement, JCGM 100:2008 (GUM 1995 with Minor Corrections) 1st edn (Sèvres: BIPM Joint Committee for Guides in Metrology).

Brusa RW, Fröhlich C, 1986: Absolute radiometers (PMO6) and their experimental characterization. Applied Optics 25, 4173-4180.

CIMO-VII 1977, WMO - Commission for Instruments and Methods of Observation, Abridged Final Report of the Seventh Session (Hamburg, 1-12 August 1977). WMO Report No. 490.

CIMO 2017. World Meteorological Organization, CIMO Guide 2017; "WMO Guide to Meteorological Instruments and Methods of Observation". Report WMO-No. 8.

Fröhlich C, London J, 1986: Revised Instruction Manual on Radiation Instruments and Measurements. World Climate Research Programme, WCRP Publications Series No. 7. WMO/TD No. 149 Report.

Fehlmann A, Kopp G, Schmutz W, Winkler R, Finsterle W, Fox N, 2012: Fourth World Radiometric Reference to SI radiometric scale comparison and implications for on-orbit measurements of the total solar irradiance. Metrologia 49, S34–S38.

Finsterle W, Blattner P, Moebus S, Rüedi I, Wehrli C, White M, Schmutz W, 2008: Third comparison of the World Radiometric Reference and the SI radiometric scale. Metrologia 45, 377-381.

Finsterle W, 2016: Final Report of the WMO International Pyrheliometer Comparison IPC-XII (2015). WMO IOM Report No.124.

Frölich C, 1991: History of Solar Radiometry and the World Radiometric Reference. Metrologia 28, 111–115.

Fox NP, Rice JP, 2005: Absolute Radiometers. In: Optical Radiometry, Experimental Methods in the Physical Sciences, Vol: 41. Parr AC, Datla RU and Gardner JL, eds. (Elsevier). pag: 35-96

Hengstberger F (editor), 1989: Absolute Radiometry (Academic Press).

Hickey JR, Frieden RG, Griffin FJ, Cone SA, Maschhoff RH, Gniady J, 1977: The self-calibrating sensor of the Eclectic Satellite Pyrheliometer (ESP) program. Proceedings of the 1977 Annual Meeting of the ASES (American Solar Energy Society), Vol 1, Sec.15-1. Boulder, CO, 6-10 June 1977.

Jung TM, Carter AC, Sears DR, Woods SI, Defibaugh DR, Kaplan SG, Zeng J, 2015: LBIR Fluid Bath Blackbody for Cryogenic Vacuum Calibrations. Conference on Characterization and Radiometric Calibration for Remote Sensing (CALCON 2015)

Karoli AR, Hickey JR, Frieden RG, 1983: Self-calibrating Cavity Radiometers t the Eppley Laboratory: Capabilities and Applications. Proceedings of the SPIE Vol.0416, Applications of Optical Metrology: Techniques and Measurements II (22 September 1983).

IPC 1980, Fifth International Pyrheliometer Comparisons and Absolute Radiometer Comparisons (IPC V), Results and Symposium. Swiss Meteorological Institute, Working Report No. 94 (1981)

IPC 1990, International Pyrheliometer Comparisons (IPC VII), Results and Symposium. Swiss Meteorological Institute, Working Report No. 162 (1991)

Neugebauer M, Schulz D, Krystek M, 2015: Calibration of circular apertures using an optical CMM. Proceedings of Euspen's 15th International Conference & Exhibition (Leuven, Belgium) 153-154

NIST 2021. NIST/SEMATECH e-Handbook of Statistical Methods: https://doi.org/10.18434/M32189. Section 2.1.1.1 (last visited on December 2022).

NREL 2021. Data of solar spectral irradiance at Air Mass 1.5 were taken from NREL webpage, Solar Resource Data and Tools. Link: https://www.nrel.gov/grid/solar-resource/spectra-am1.5.html (last visited on January 2022).

Patrick HJ, Germer TA, Zarobila CJ, Cooksey CC, Yoon HW, 2016: Optical Reflectance of Pyrheliometer Absorption Cavities: Progress Toward SI-traceable Measurements of Solar Irradiance. Applied Optics 55, 6346–6354

Romero J, Fox NP, Fröhlich C, 1991: First Comparison of the Solar and an SI Radiometric Scale. Metrologia 28, 125–128

Romero J, Fox NP, Fröhlich C, 1995: Improved comparison of the World Radiometric Reference and the SI radiometric scale. Metrologia 32, 523-524.

Zerlaut GA, 1982: Solar Radiation Measurements: Calibration and Standardization Efforts. In: Advances in Solar Energy (Boer KW, Duffie JA, eds), Vol.1, pp.19-60. American Solar Energy Society.